

Measurement of p^\uparrow Au and p^\uparrow d Analyzing Power in CNI region at RHIC Hydrogen Jet Polarimeter*

A.A. Poblaguev,[†] E. Aschenauer, G. Atoian, K.O. Eyser,
H. Huang, Y. Makdisi, W. Schmidke, G. Webb, and A. Zelenski
Brookhaven National Laboratory, Upton, New York 11973, USA

I. Alekseev and D. Svirida

Institute Theoretical and Experimental Physics (ITEP), 117259 Moscow, Russia

(Dated: January 19, 2017)

In 2016 Deuterium-Gold beams energy scan at RHIC, we employed Hydrogen Jet Polarimeter (HJET) to measure analyzing power of polarized proton scattering on Deuterium and Gold. The experiment was performed in parallel with the main RHIC program. The measurements were done in the $0.002 < -t < 0.020$ (GeV/c)² momentum transfer range at 4 beam energies 9.8, 19.5, 31.2, and 100.3 GeV/n. The sources of systematic errors are discussed. Preliminary results for similar measurements of proton scattering on p, Au, and Al at 100 GeV obtained in RHIC Run15 are also presented.

I. INTRODUCTION

A spin correlated asymmetry in elastic scattering of transversely polarized proton on unpolarized target may be parametrized as

$$\frac{d^2\sigma}{dt d\varphi} = \frac{1}{2\pi} \frac{d\sigma}{dt} [1 + A_N(t)P \sin \varphi] \quad (1)$$

where φ is angle between vectors of incident proton spin and transverse momentum of scattered proton, P is the beam proton polarization, and $A_N(t)$ is analyzing power.

The asymmetry A_N originates from interference of spin-flip and non-spin-nonflip amplitudes of proton-nucleus scattering. Experimental study of $A_N(t)$ in high energy proton scattering on nucleus at low momentum transfer (Coulomb-nuclear interference region, CNI) is interesting because (i) it involves application of QCD in a kinematical region where non-perturbative effects are important [1] and (ii) detailed understanding of analyzing power is essential for polarimetry, e.g. at RHIC [2].

In 2016, RHIC operation included 5 weeks of Deuterium-Gold energy scan at 4 beam energies (E_{beam}) 9.8, 19.5, 31.2, and 100.3 GeV/n [3]. We used this opportunity to measure $p^\uparrow d$ and p^\uparrow Au analyzing power. The measurements were done with HJET polarimeter [4] in a background mode, i.e. in parallel with the main RHIC program. Scattering of the beam nucleus with energy E_{beam} on the polarized proton target is equivalent to the scattering of proton with energy

$$E_p = E_{\text{beam}} \frac{m_p N}{M} \approx E_{\text{beam}} \quad (2)$$

on the nucleus in rest. Here, m_p is proton mass, M is nucleus mass, and N is number of nucleons in the nucleus.

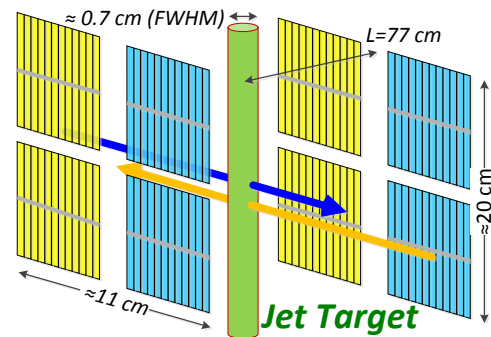


FIG. 1. A schematic view of HJET polarimeter. 8 Silicon detectors, 12 readout channels each, are optionally referred as *blue* and *yellow* depending on which RHIC beam they measure.

II. HJET POLARIMETER

HJET polarimeter, commissioned in 2004, was designed to measure absolute polarization of 24-250 GeV/c proton beams at RHIC with systematic errors better than $\Delta P/P \lesssim 0.05$. The main HJET components are Polarized Atomic Hydrogen Gas Jet Target, Breit-Ruby polarimeter to measure hydrogen atoms polarization, and recoil spectrometer. Both RHIC beams, *blue* (Deuterium in Run 16) and *yellow* (Gold), are measured simultaneously. The polarimeter geometry is sketched in Fig. 1.

The nuclear polarization of the hydrogen atoms in the jet, $P_{\text{jet}} = 0.958 \pm 0.001$, is known with a high accuracy. The jet density profile in horizontal direction is well approximated by Gaussian distribution ($\sigma \approx 2.6$ mm) with 1.2×10^{12} atoms/cm² in the center. In the measurements, the jet polarization is reversed every 5 minutes.

To detect recoil protons, we use 8 pairs of Si wafers (12 vertically oriented strips of 3.75×45 mm² size, 470 μ m thickness, ~ 0.37 mg/cm² uniform dead-layer). For elas-

* Work supported by the US Department of Energy under contract number DE-SC0012704. Funding was also provided from the RIKEN BNL Research Center.

[†] poblaguev@bnl.gov

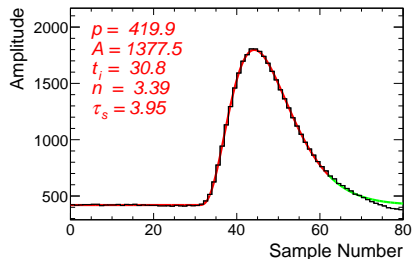


FIG. 2. Signal waveform in HJET (black histogram). The red line indicates the time interval which is used in the waveform fit. The green line is the waveform function $W(t)$ beyond this interval. The sample time is about 4.1 ns.

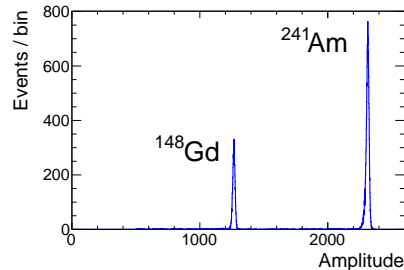


FIG. 3. Signal amplitude distribution in the α -source calibration.

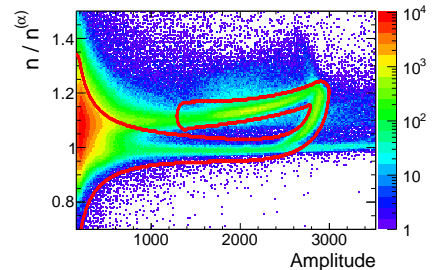


FIG. 4. Event selection cut (solid red line) to separate punched-through and stopped protons for the $0.5 < T_R < 13$ MeV energy range. No other cuts had been applied in this plot.

tic scattering, the spectrometer geometry allows us to detect recoil protons with kinetic energy up to $T_R \approx 10$ -11 MeV which corresponds to momentum transfer $-t = 2m_p T_R \lesssim 0.020$ (GeV/c) 2 . Protons with energy above 7.8 MeV punch through the Si detector (only part of the proton kinetic energy is detected).

For signal readout we use 12 bit 250 MHz FADC250 wave-form digitizers [5]. A full waveform (80 samples) is recorded for every signal above ~ 0.5 MeV threshold (Fig. 2). In the data analysis, the signal shape was parametrized by the following function

$$W(t) = p + A(t - t_i)^n \exp\left(-\frac{t - t_i}{\tau_s}\right) \quad (3)$$

The maximum amplitude time t_m is related to the signal start time t_i as $t_m = t_i + n\tau_s$.

III. ENERGY CALIBRATION OF SI DETECTORS

For energy calibration, all Si strips are exposed by α -particles from two sources, ^{148}Gd (3.183 MeV) and ^{241}Am (5.486 MeV). A typical signal amplitude distribution in a Si strip is shown in Fig. 3.

Two different energies of α -particles allows us to determine both gain $g \sim 2.5$ keV/cnt and dead-layer thickness $x_{\text{DL}} \sim 0.37$ mg/cm 2 in every Si strip. Energy resolution $\sigma_E \sim 20$ keV is dominated by electronic noise.

To separate punched-through and stopped protons with the same measured signal amplitude we analyzed the waveform shape. For that, the dependence of signal amplitude A and waveform shape parameters n and τ_s on proton kinetic energy T_R was simulated [7, 8]. The simulation parametrization was adjusted using α -calibration data. For every pair of measured parameters A and n (within good event selection cut) the corresponding recoil proton kinetic energy was determined. The A - n based event selection is illustrated in Fig. 4, $n^{(\alpha)}$ is the waveform shape parameter n measured in α -calibration.

IV. EVENT SELECTION

A typical measured time-amplitude distribution in a silicon strip is shown in Fig. 5. To study spin correlated asymmetries we have to isolate elastic events.

First, we have to verify that detected particle is a proton. For that, we compare the measured signal time t with expected time for recoil proton kinetic energy T_R (derived from measured amplitude A)

$$\delta t = t - t_0 - \text{tof} = t - t_0 - \frac{L}{c} \sqrt{\frac{m_p}{2T_R(A)}} \quad (4)$$

Here, $L = 769$ mm is the distance to detector, c is speed of light, and t_0 is the time offset. Since the δt distribution is dominated by the beam bunch longitudinal profile, it is expected to be the same for all Si strips.

Second, we have to verify that missing mass M_X (the effective mass of the scattered particles) is equal to the beam particle mass M . This condition may be written as

$$z_{\text{strip}} - z_{\text{jet}} = L \sqrt{\frac{T_R}{2m_p} \frac{E_p + m_p^2/M}{E_p - m_p + T_R}} = \kappa \sqrt{T_R} \quad (5)$$

Here, z_{strip} and z_{jet} are z -coordinates of recoil proton in the detector and in the jet (scattering point), respectively. For elastic scattering, the event rate dependence on recoil proton energy can be described as

$$dN/d\sqrt{T_R} \propto \sqrt{T_R} (d\sigma/dt)_{el} f(\kappa\delta\sqrt{T}) \quad (6)$$

where $f(z)$ is jet target density profile and

$$\delta\sqrt{T} = \sqrt{T_R} - \sqrt{T_{\text{strip}}} \quad (7)$$

Here, T_{strip} is recoil proton energy corresponding to the strip center ($\kappa\sqrt{T_{\text{strip}}} = \langle z_{\text{strip}} \rangle - \langle z_{\text{jet}} \rangle$). Since the $\delta\sqrt{T}$ distribution is dominated by the jet density profile it has to be the same for all Si strip. If so, it is convenient to use the $\delta\sqrt{T}$ for elastic event selection cut.

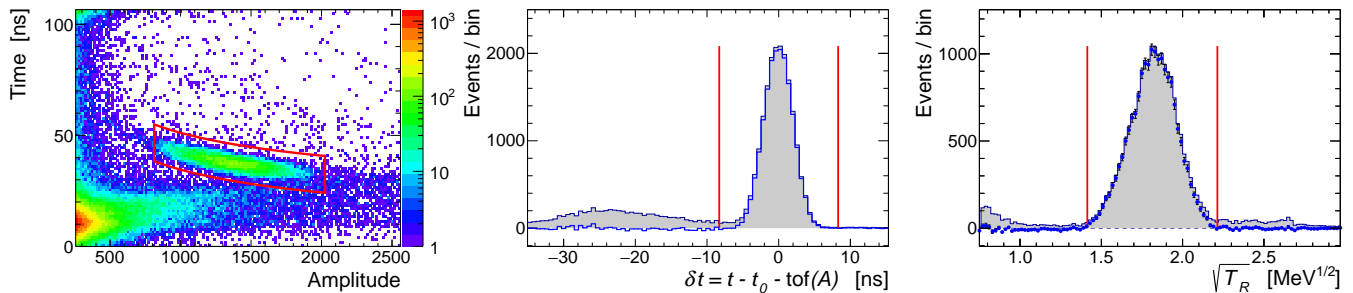


FIG. 5. Elastic event isolation in blue detector in the 10 GeV dAu run. Event selection cuts are show by red lines. The $\delta\sqrt{T}$ cut is applied for events in the δt histogram, and the δt cut is applied in the T_R histogram.

The efficiency of this cut may be affected by detector misalignment during installation and by corrections $\sim b_{MF}/\sqrt{T_R}$, $|b_{MF}| \lesssim 1 \text{ mmMeV}^{1/2}$ due to recoil proton track bending in the holding magnetic field. A method to evaluate these corrections with accuracy $\sim 100 \mu\text{m}$ was developed [6, 8]. However, for our current understanding of HJET geometry and the holding magnetic field, we observe a discrepancy which may be described as a possible correction to the measured kinetic energy,

$$\Delta\sqrt{T_R} \approx 0.035 + 0.009\sqrt{T_R}, \text{ MeV}^{1/2} \quad (8)$$

Since the source of discrepancy is not identified yet, we currently have to interpret the Eq. (8) as a possible systematic error $\langle\Delta T/T\rangle \approx 3\%$ or $\langle\Delta T\rangle \approx 0.18 \text{ MeV}$ in a recoil proton kinetic energy measurement.

V. SPIN DEPENDENT ASYMMETRIES

Number of events detected in left/right detectors (relative to the beam direction) depending on the jet polarization ($\uparrow\downarrow$) may be approximated as

$$N_{LR}^{\uparrow\downarrow} \propto (1 + \eta^{\uparrow\downarrow} \eta^{LR} P_{\text{jet}} \langle A_N \rangle) \cdot (1 + \eta^{LR} \varepsilon) \cdot (1 + \eta^{\uparrow\downarrow} \lambda) \quad (9)$$

where $\langle A_N \rangle$ is average analyzing power in the measurement, ε is left/right acceptance asymmetry, λ is up/down

luminosity asymmetry, and η^{ab} equals to $+1$ if a and -1 if b . Equations (9) have an exact solution

$$P_{\text{jet}} \langle A_N \rangle = \frac{\sqrt{N_L^\uparrow N_R^\downarrow} - \sqrt{N_R^\uparrow N_L^\downarrow}}{\sqrt{N_L^\uparrow N_R^\downarrow} + \sqrt{N_R^\uparrow N_L^\downarrow}} \quad (10)$$

and similar expressions for λ and ε . Actually this is a systematic error free measurement of analyzing power if $\langle A_N \rangle$ is the same for left/and right detectors, acceptance asymmetry ε does not depend on the spin direction, and $\delta P = |P_{\text{jet}}^\uparrow| - |P_{\text{jet}}^\downarrow| = 0$. However even in this case we actually measure only *effective* analyzing power which is generally modified by background and/or errors in energy calibration

$$\delta A_N = \frac{b}{1+b} \left(A_N^{(\text{bgr})} - A_N \right) - 2m_p \frac{dA_N(t)}{dt} \delta T_R \quad (11)$$

where b is background to signal ratio and $A_N^{(\text{bgr})}$ is effective analyzing power for background events. In most cases, $A_N^{(\text{bgr})} = 0$ for the jet polarization asymmetry. Actually, δA_N may be considered as a systematic error in definition of the analyzing power. Generally, it is not the same for left and right detectors.

In a first order approximation, systematic errors in

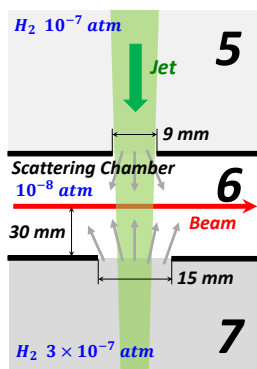


FIG. 6. Molecular hydrogen flow in HJET.

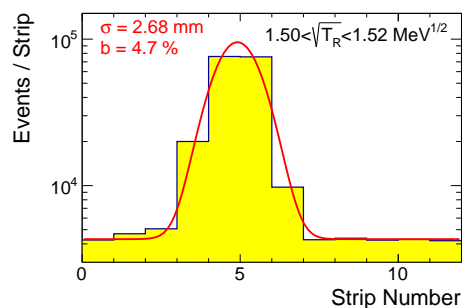


FIG. 7. The jet density profile measured by histogramming good events rate in Si strips of one detector. b is the flat background to elastic signal ratio in the jet center.

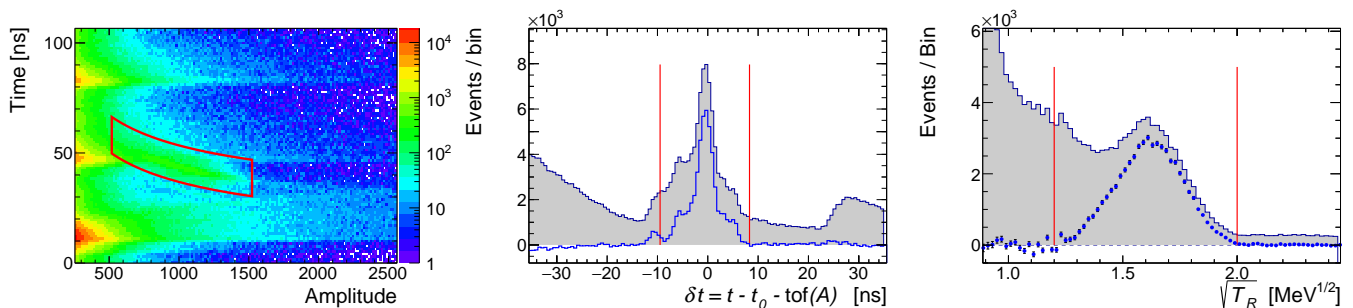


FIG. 8. Background subtraction in very high background data. The gray filled histograms shows event distributions before background subtraction, the blue histograms are distributions after subtraction. Red lines show event selection cuts.

asymmetry measurements may be summarized as

$$P_{\text{jet}} \delta A_N^{\text{syst}} = P_{\text{jet}} \frac{\delta A_N^{(L)} + \delta A_N^{(R)}}{2} + \frac{\delta \varepsilon_L - \varepsilon_R}{2} \quad (12)$$

$$\delta \lambda^{\text{syst}} = P_{\text{jet}} \frac{\delta A_N^{(L)} - \delta A_N^{(R)}}{2} + \frac{\delta \varepsilon_L + \varepsilon_R}{2} \quad (13)$$

where $\delta A_N^{(L,R)}$ and $\varepsilon_{L,R}$ are average corrections in left/right detectors for analyzing power and for acceptance dependence on the jet polarization, respectively. If only one of the corrections $\delta A_N^{(L,R)}$, $\delta \varepsilon_{L,R}$ is non-zero, there is a strict correlation between systematic errors in measurement of analyzing power A_N and luminosity asymmetry λ . Since the measured $\lambda(t)$ has to be independent of recoil proton energy T_R , the measured $\lambda(T_R)$ dependence may provide an evaluation of systematic errors in the analyzing power measurements.

VI. BACKGROUND

In HJET, two main sources of background are contamination of the jet by hydrogen atoms bound into unpolarized proton molecule (molecular hydrogen) and beam scrapping (here, the beam scattering on any non-proton targets).

As it shown in Fig. 6, molecular hydrogen fills the scattering chamber 6 by diffusion from the Chamber 7 (scattered and recombined jet atomic hydrogen) and Chamber 5 (unfocused hydrogen atoms recombined to molecules). We can expect that density profile for molecular hydrogen is much larger than for the atomic hydrogen in the jet. Such a wide spatial distribution allows us to properly account the molecular hydrogen and subtract it from the jet data.

As it follows from Eq. (5), for elastic scattering and fixed recoil energy T_R , the events distribution in silicon strips of one detector (see Fig. 7) is just a histogram of the longitudinal profile of the jet density. Contribution from scrapping events is also expected to has flat distribution in Fig. 7 because detector's acceptance angle is small and there is no strict correlation between recoil proton kinetic energy and direction.

As result, all background, except for molecular hydrogen in the jet core, is expected to have flat distribution in Fig. 7 and, thus, may be subtracted using standard methods. For every detector, the background rate may be determined as a function of δt and T_R . To account properly possible spin correlated effects associated with background it has to be evaluated separately for every polarization state. The results of background subtraction is demonstrated in Fig. 8. For illustration purposes we used data with unusually high background level. Even in this case the method works well. Inspecting the results of background subtraction we found that inaccuracy of background subtraction does not exceed 10% of the background level which means a dilution to a sub-percent level of the residual background contribution to the elastic data.

VII. SYSTEMATIC ERRORS

A. Noise dependence on the jet polarization

It was found in RHIC Run 15 (pp , 100 GeV) data analysis that the HJET negative polarization cavity induces significant electronic noise in one *blue* detector [8]. This noise affects the efficiency of event selection cuts (especially for low T_R) and results in a non-zero contribution $\varepsilon_L > 0$ to Eqs. (12,13). By optimizing the cuts, this systematic error was strongly suppressed and was actually observed only for $T_R \lesssim 1$ MeV. In Run 16, the effect was significantly suppressed, but not totally eliminated. We do not expect and do not observe, in a glance, any visible systematic errors associated with this noise. However an exhaustive study has not been carried out yet.

B. Molecular hydrogen background

A special study of molecular hydrogen distribution was performed in Run 16. The jet was turned off and molecular hydrogen background was emulated by injection of hydrogen gas to the Chamber 7. The test run was taken

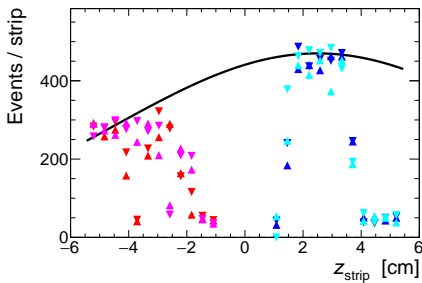


FIG. 9. Event rate distribution in measurements with hydrogen injected to the Chamber 7. The jet was off. Markers' styles/colors denote different Si detectors.

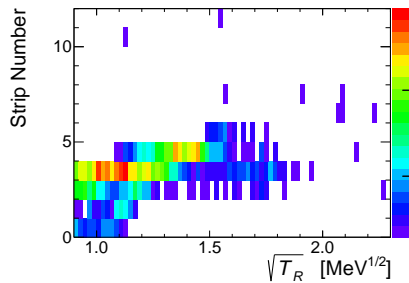
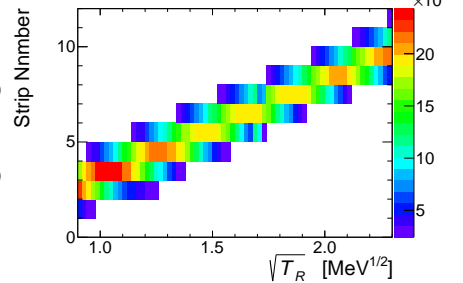


FIG. 10. Event rate distribution in blue left bottom detector in the empty target(left) and regular(right) runs.



with a single (blue) Gold beam. The event rate distribution (the molecular hydrogen profile) in all Si strips is shown in Fig. 9. The molecular hydrogen density may be approximated by a Gaussian distribution (solid black line), about 30 times wider compared to the jet density profile. It means the almost flat distribution of molecular hydrogen background in Fig. 7. However, the distribution in Fig. 9 is strongly shadowed by collimators in HJET construction. The normalization of the molecular hydrogen distribution was done by two methods (i) by comparing pressure in the scattering chamber in the test and in a regular data taking runs and (ii) by searching in regular runs a bump seen in yellow detectors ($z_{\text{strip}} < 0$) in Fig. 9. Both methods gave consistent results of $b_{\text{MH}} = 0.9 \pm 0.3\%$ for integrated molecular hydrogen contamination in the jet. The actual event selection cut of $|\delta\sqrt{T}| < 0.4 \text{ MeV}^{1/2}$ was accounted in this value. Due to collimators, only $\delta b_{\text{MH}} = 0.3 \pm 0.1\%$ of the molecular hydrogen contamination was actually subtracted in the data analysis. In a similar way we also evaluated that molecular hydrogen contribution (coming directly from the dissociator) in the jet core is $b_{\text{MH}} = 0.4 \pm 0.2\%$. In the data analysis, the molecular hydrogen background may be accounted by a correction to the jet polarization value. Summarizing, the effective hydrogen polarization in the jet was estimated as

$$P_{\text{jet}}^{(\text{eff})} = P_{\text{jet}} / (1 + b_{\text{MH}}) = 94.8 \pm 0.5\% \quad (14)$$

C. Beam Scrapping

Another collimator related issue was found in an empty target (jet off) run. In this case, only scrapping background is detected and we could expect the same rate in all Si strips. This assumption was clearly violated in blue left detectors (see Fig. 10). Since the observed energy/strip distribution is strongly overlapped with the elastic scattering distribution, this background is not being subtracted. The situation may be described by a correction $\delta A_N^{(\text{R})} < 0$ in Eqs. (12,13) which results in

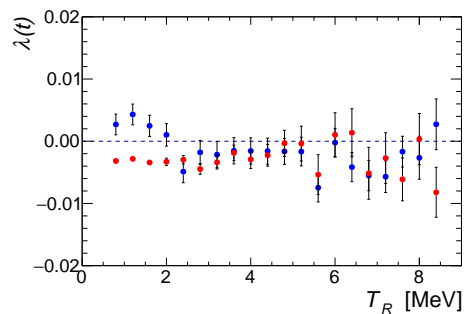


FIG. 11. Measured $\lambda(t)$ asymmetry for Deuterium (blue) and Gold (red) in the 10 GeV/n run. The discrepancy for $T_R < 3 \text{ MeV}$ can be attributed to the beam scrapping background (VII C).

correlated systematic errors

$$\delta A_N^{\text{syst}}(t) = -\delta\lambda^{\text{syst}}(t) \quad (15)$$

for low $T_R < 2.5 \text{ MeV}$ recoil proton energies. The measured dependence $\lambda(t)$ shown in Fig. 11 clearly indicates the contribution of this background to the $p^\uparrow d$ results at low momentum transfer. Comparing the measured $\lambda(t)$ for Deuterium beam with the average value at $T_R > 3 \text{ MeV}$ we can calculate systematic error corrections to the measured analyzing power.

D. Inelastic Scattering

A possible contribution of inelastic scattering

$$p^\uparrow A \rightarrow p + X, \quad M_X = M + \Delta \quad (16)$$

requires a special consideration. In HJET, such a process may manifest itself by increasing recoil proton angle (5)

$$\kappa \rightarrow \kappa \times \left(1 + \frac{2m_p\Delta}{T_R E_p} \right) \quad (17)$$

For 100 GeV, HJET geometry does not allow us to detect inelastic processes if $\Delta > 150 \text{ MeV}$. For 10 GeV beam

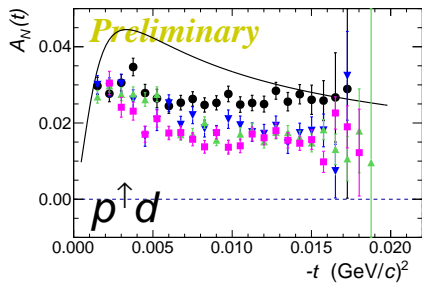


FIG. 12. Preliminary results for measurements of $p^\uparrow d$ and $p^\uparrow \text{Au}$ analyzing power at 9.8 (●), 19.5 (▼), 31.2 (▲), and 100.3 (■) GeV. Only statistical errors are shown. The $A_N(t)$ theoretically calculated (with no hadronic spin-flip) for elastic $p^\uparrow p$ scattering at 100 GeV is shown by black lines to define the scale.

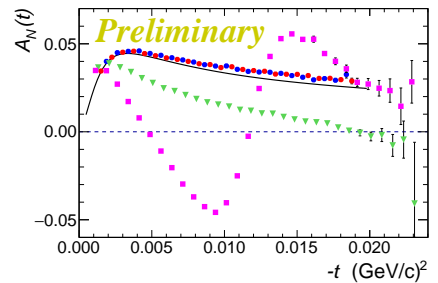
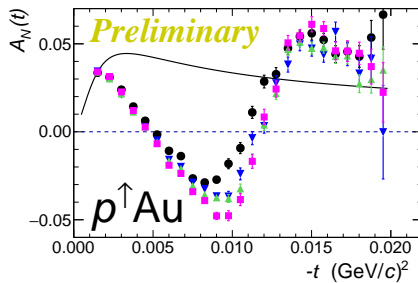


FIG. 13. Preliminary results for $p^\uparrow p$ (● and ● for blue and yellow beams, respectively), $p^\uparrow \text{Al}$ (▼), and $p^\uparrow \text{Au}$ (■) analyzing powers measured with 100 GeV/ n beams in RHIC Run15.

this threshold is ~ 15 MeV. The detected inelastic events may be indicated by an excess of background events in Si strips with high numbers in the jet profile distribution in Fig. 7. Inspecting such histograms we did not find any evidence of inelastic events at a 0.3% level.

However, it should be pointed out that the used method is not sensitive to “quasi-elastic” processes with small Δ . Possible sources of such processes are proton scattering on spectator nucleon in the nucleus [9] and photonuclear reactions [10]. An accurate measurement of parameter κ may indicate such a background. At a first look, we can not exclude $\langle \Delta \rangle \sim 1$ MeV for Deuterium data. However, more study is still needed for a confident conclusion.

VIII. RESULTS

Preliminary results of measurement of analyzing power for $p^\uparrow d$ and $p^\uparrow \text{Au}$ elastic scattering at 9.8, 19.5, 31.2, and 100 GeV/ n are given in Fig. 12. Only statistical errors are shown. For Deuterium, the systematic error correction was applied at low T_R as described above. From analysis of fluctuation in $\lambda(t)$ we estimated an upper limit for systematic errors in every measured point as $\sigma^{\text{syst}} \lesssim 0.002$. Possible systematic errors in determination of $-t = 2m_p T_R$ were discussed in section IV.

One can see that $p^\uparrow d$ analyzing power for 10 GeV/ n is significantly different compared to 20-100 GeV/ n . For $p^\uparrow \text{Au}$ the analyzing power is almost independent of the beam energy for $-t < 0.005$ (GeV/ c)² but strongly beam energy dependent for $-t \sim 0.010$ (GeV/ c)². It is also interesting to note that proton-Gold $A_N(t, E_p)$ dependencies have some common features with the $p^\uparrow p$ scattering [11] (however with significantly different $-t$ scale).

For comparison, preliminary results for $p^\uparrow p$, $p^\uparrow \text{Al}$, and $p^\uparrow \text{Au}$ analyzing power measured in RHIC Run15 at 100 GeV are shown in Fig. 13. The horizontal 4.8 mrad angle for Al and Au beams allowed us to extend the momentum transfer range. However for large $-t$, the recoil protons were detected only in the left detectors and asymmetry was calculated simply by comparison statistics with jet spin up and down. A required corrections due to luminosity asymmetry λ were determined using data with 3-8 MeV recoil protons.

To complete this experimental study we still need (i) to resolve an issue with energy calibration, (ii) to optimize separation of punched-throw and stopped recoil protons, (iii) to make evaluation of contribution of inelastic events, (iv) investigate a possibility of parametrization of elastic cross-section $d\sigma/dt$ in these measurement, and (v) routinely check all data for possible detector instabilities during the measurements. We are also awaiting for new theoretical parametrization for proton-Gold scattering [12].

[1] B. Z. Kopeliovich and T. L. Trueman, Phys. Rev. D **64**, 034004 (2001); T. L. Trueman, Phys. Rev. D **77**, 054005 (2008).
[2] I. Nakagawa *et al.*, Eur. Phys. J. ST **162**, 259 (2008).
[3] C. Liu *et al.*, BNL-113241-2016-IR (November 2016),
[4] A. Zelenski *et al.*, Nucl. Instrum. Meth. A **536**, 248 (2005); H. Okada *et al.*, Phys. Lett. B **638**, 450 (2006); I. G. Alekseev *et al.*, Phys. Rev. D **79**, 094014 (2009).
[5] H. Dong *et al.*, 2007 IEEE Nuclear Science Symposium Conference Record, Honolulu, HI, 2007, pp. 831-833.

doi:10.1109/NSSMIC.2007.4436457.
[6] A. Poblaguev, BNL-104-363-2014-IR (March 2014),
[7] A. Poblaguev, BNL-104-366-2014-IR (February 2014),
[8] A. Poblaguev, PoS PSTP **2015**, 032 (2015).
[9] V.V. Glagolev *et al.*, Cent. Eur. J.Phys. **6** (2008) 781.
[10] R. E. Mikkelsen, A. H. Sørensen and U. I. Uggerhøj, Nucl. Instrum. Meth. B **372**, 58 (2016)
[11] O. V. Selyugin, Phys. Part. Nucl. Lett. **13**, no. 3, 303 (2016).
[12] B. Z. Kopeliovich, private communication.